RADARSAT-1 Doppler Centroid Estimation Using Phase-Based Estimators

Ian Cumming[(1)], Frank Wong[(2)] and Bob Hawkins[(3)]

(1) Remote Sensing Data Centre (DFD)
Deutschen Zentrum fur Luft und Rahmfahrt (DLR)
Postfach 1116, D-82234 Wessling, Germany. Ian.Cumming@dlr.de

(2) The National University Of Singapore
Electrical Engineering, 10 Kent Ridge Crescent, Singapore 119260
Email: elewongf@nus.edu.sg

(3) Canada Centre For Remote Sensing
Data Acquisition Division, 588 Booth St, Ottawa, Canada K1A 0Y7
Email: Robert.Hawkins@ccrs.nrcan.gc.ca

ABSTRACT[1]: — When processing satellite SAR scenes in a production environment, it has been found that image quality distortions (radiometric, geometric, and phase) that occur in a few percent of the scenes can be traced to errors in the Doppler centroid (DOPCEN) estimators. Radiometric scalloping is particularly an issue with ScanSAR scenes as they have more sensitive DOPCEN tolerances.

In this paper, we examine some troublesome RADARSAT-1 scenes, in which Doppler centroid estimation errors are frequently caused by radiometric discontinuities in the scene. After reviewing the operation and performance of several current Doppler estimators, we propose a scheme based on a spatial diversity concept, in which areas that cause poor estimates are removed from the estimation process.

1 Introduction

Doppler Centroid (DOPCEN) estimation continues to be an important [1] and sometimes overlooked component of SAR processing. The issue is especially acute in the case of RADARSAT-1 ScanSAR processing, where the estimate must be accurate to approximately 5 Hz in order to avoid radiometric artifacts such as scalloping in the processed images [2].

In the last 10 years, a new class of estimator has been developed based on the phase of the received signal, rather than on the spectral amplitude. The concepts were developed by Madsen [3], Bamler and Runge [4], and more recently by Wong and Cumming [5]. It is generally acknowledged that the phase-based estimators can be more accurate than the amplitude-based estimators, provided their limitations are understood, and they are applied properly.

We consider the DLR [4], the MLCC and the MLBF [5] algorithms, as well as the classic spectral-fit algorithm. We have found that their performance differs as a function of radiometric discontinuities, partially-exposed targets, noise levels, and scene contrast.

In this paper, we review the operation of the DOPCEN algorithms, compare their performance, explain why it is advantageous to combine estimates from more than one algorithm, and propose a new estimation scheme that uses spatially diverse parts of the scene to obtain reliable estimates.

2 Review of Estimators

In this section, we will review the algorithms used in the most common DOPCEN estimators. Because of space limitations, we will concentrate on estimates of the "fractional-PRF" part of the Doppler centroid. Obtaining a good fractional-PRF estimate is a prerequisite to obtaining a good Doppler ambiguity estimate, and in many cases, the associated Doppler ambiguity estimator has similar estimation properties with respect to data anomalies.

2.1 Classic spectral amplitude fit

This was the first DOPCEN estimator [6] used for satellite SAR data, and is still in common use. The shape of the azimuth magnitude spectrum is averaged over a suitable range/azimuth window, and compared with the expected shape based on the azimuth beam pattern and received SNR [6, 7]. A correlation is done between the measured and modelled azimuth spectrum to determine the Doppler frequency of the peak of the measured spectrum. Accuracies are typically a few tens of Hz when a million samples are analyzed.

[1]Presented at the CEOS'99 SAR Workshop, Toulouse, October 26-29, 1999. Dr. Cumming is currently on sabbatical leave from the University of British Columbia (ianc@ece.ubc.ca). Dr. Wong is currently on leave of absence from MacDonald Dettwiler and Associates.

2.2 Phase increment methods

In 1989, Madsen recognized that the centroid could be measured by finding the average phase increment in the azimuth data [3]. Later, Bamler and Runge of DLR, and Wong and Cumming applied the same principle to Doppler ambiguity resolvers [4, 5]. We refer to the latter algorithms as the DLR and the MLCC (for Multi-Look Cross-Correlation) algorithms.

Considering a point target, the change in phase between one azimuth sample and the next varies linearly with time along the exposure of the target, as shown in the top panel of Fig. 1. In the bottom panel, we show the individual phase increments in the complex plane, going from the beginning of the exposure A to the end B. We also show their vector sum (the longer vector with the circle at its end). Since the target is strongest at the Doppler centroid, and its exposure is symmetrical about the centroid; finding the average phase increment (vector sum) along the whole exposure will then give the Doppler centroid. A target which is only partially exposed in the estimation window (or any other non-symmetry in the exposure) will bias the estimate. Accuracies of the phase increment methods are generally a little better than the classic method.

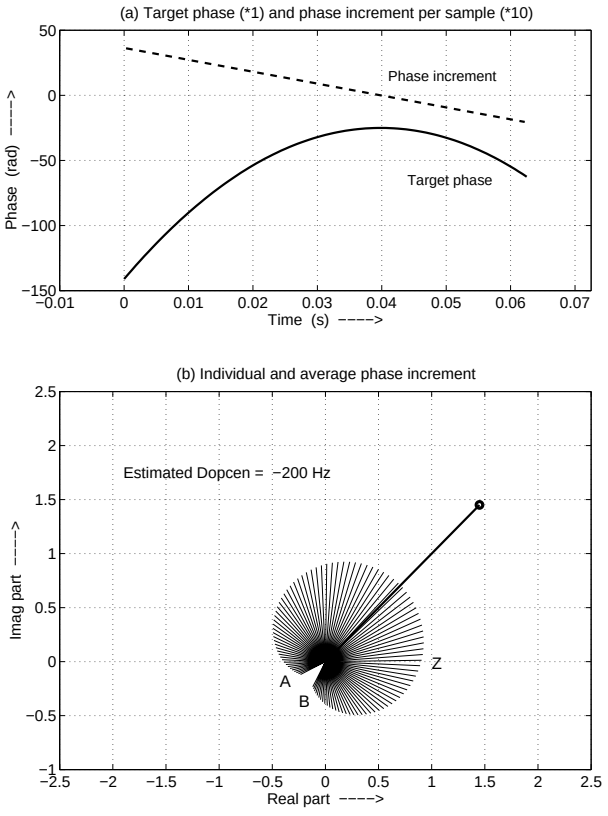

Figure 1: Principles of phase increment methods.

2.3 MLBF algorithm

Wong and Cumming developed an additional method of finding the Doppler ambiguity when a colleague at MacDonald Dettwiler, Robert Deane, recognised that the beat frequency formed by multiplying the received signal from radar systems of slightly different centre frequencies was proportional to the unaliased Doppler centroid [8]. The different radar frequencies are obtained by extracting two looks from the range spectrum. The method is not accurate enough to estimate the fractional-PRF centroid to a useful accuracy, but it is generally accurate enough to estimate the ambiguity.

3 RADARSAT-1 Data

We investigated four RADARSAT-1 scenes which had DOPCEN estimation errors. They all had severe azimuth radiometric discontinuities. An example is the standard beam 7 scene shown in Fig. 2. The scene is centred at 49.94^o N, 63.09^o W, and the data were collected on the 142nd day of 1996, at 10:13:15 UTC. The spacecraft heading was 195.6^o (descending orbit). The scene contains part of the north shore of the St. Lawrence River in eastern Canada (top) and Anticosti Island (bottom). The bright land beside the dark water creates a radiometric discontinuity of up to 16 dB.

Also noted in the left of the scene is a darkening of a portion of the land area caused by raw data saturation. This occurs because the Automatic Gain Control (AGC) scheme adopted for RADARSAT-1 measures the signal strength in the first quarter of the range swath [9], and cannot adapt to the bright land in the far range (left) part of the scene with the four bits available. This artifact, which is not uncommon in coastal scenes, presents a special DOPCEN estimation case.

3.1 What upsets estimators

If the radar SNR is high enough, and equal-strength targets are spread uniformly throughout the estimation window, then most DOPCEN estimators give excellent results. In examining scenes which gave poor Doppler estimates, the following scene characteristics were identified as having a possible effect upon the estimation accuracy:

- Azimuth radiometric discontinuities
- Range radiometric discontinuities
- The level of scene contrast
- Low SNR

It was soon found, as indicated in Section 4.2, that azimuth radiometric discontinuities were the most troublesome. We concentrate on these in this paper.

Figure 2: RADARSAT-1 Anticosti scene (beam S7) ©CSA.

4 Initial Estimator Tests

Most estimators work on a block basis, e.g. on 4096×4096 samples. To examine the behaviour of the estimators on different scene features, we divided the scene of Fig. 2 into relatively small blocks (256×1024 samples or 4.1 km in range by 5.2 km in azimuth), and applied the estimators to each block individually. The data were range compressed but not azimuth compressed. This is the point in the SAR processing flow where the DOPCEN estimation is usually carried out.

4.1 Measuring scene statistics

Before running the estimators, we measured the radiometric gradients, the spectral distortion, the energy (SNR) and the contrast of each block. The range and azimuth radiometric gradients are shown in Fig. 3, where the prominent edges of the land/water boundaries are clearly seen. To observe the SNR and the spectral distortion, it is useful to plot the azimuth magnitude spectra averaged over each block. In Fig. 4, the spectra of azimuth block numbers (rows) 17–24 are plotted, taken down the left-hand side in Fig. 3 (range block (column) 28). Low signal strength can be observed in rows 21–24, and spectral distortion can be seen in row 20.

4.2 Simulation tests

The estimators were first tested on simulated data. Millions of point targets were used to simulate different scene contrasts and radiometric discontinuities [10].

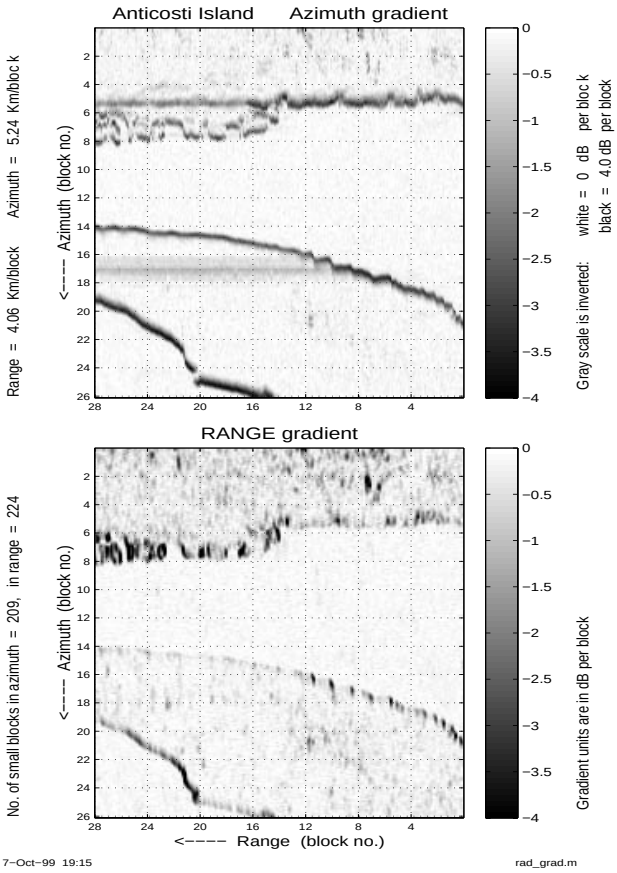

Figure 3: Range and azimuth radiometric gradients of range compressed Anticosti scene.

Simulated data were first tested with different levels of contrast by inserting strong targets between average strength targets. It was found that the DLR and MLCC algorithms worked best with low contrast scenes in which the data are more uniform and the azimuth spectrum is undistorted. In low contrast scenes, partial exposures are not so damaging, as the partially-exposed targets at the start of the estimation window are compensated by others of similar strength at the end of the window.

On the other hand, the MLBF algorithm was found to work best on scenes with high contrast. In fact, the MLBF algorithm works best when only one dominant target is present in each range cell when the beat frequency is clearest. When many targets of roughly equal strength exist in a range cell, they mix with one another and the beat frequency becomes 'smeared out'. The MLBF algorithm is not as sensitive to partial exposures, as the beat frequency does not change so much along the target's exposure.

When uniform scenes were simulated, but with range and azimuth radiometric discontinuities, it was found that the range discontinuities had little effect on es-

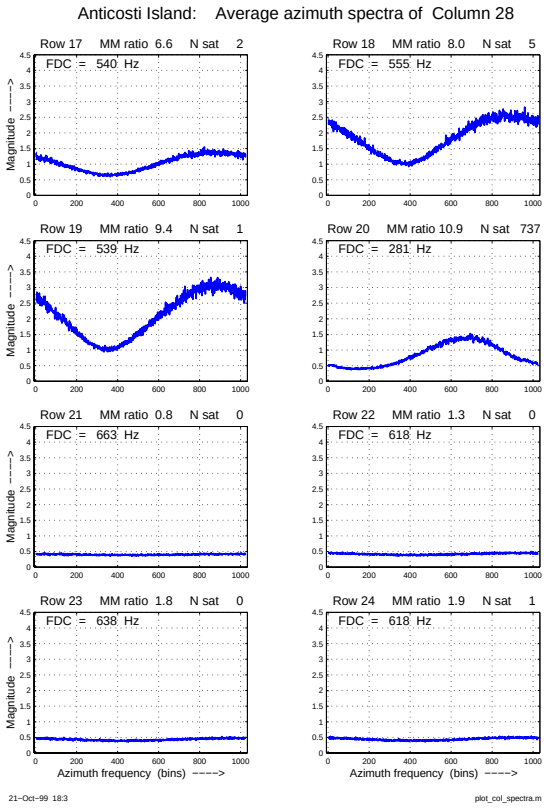

Figure 4: Azimuth spectra of column 28 of the Anticosti scene.

timator performance. However, the azimuth discontinuities had a pronounced effect on the estimators, particularly with the classic, DLR and MLCC estimators. When the data SNR was low, the standard deviation of the estimates increased, but the estimates were not biased as long as the spectrum was symmetrical. Because of the different sensitivities to scene features, we recommend running the complementary MLCC and MLBF algorithms in parallel, and using statistical quality measures to select the best estimate [5].

Based on these tests, it was determined that the major impact on the estimators was caused by partial azimuth exposures. Partial exposures occur when a strong target is present, but only part of the target is present within the estimation window.

4.3 RADARSAT-1 data tests

The 256×1024 sample data blocks were arranged in 26 rows and 28 columns, as indicated by the annotation in Fig. 3. This was convenient to run the estimators down columns or across rows, to allow unwrapping of estimates where necessary, and to provide a useful display format.

Figs. 4 and 5 show a typical set of results, when the estimators were run on the blocks going down column 28 (the left hand column). This column spans a representative set of radiometric discontinuities and we can observe the estimator behaviour on these scene features. In this case, the spectral fit estimator was used.

The upper panel of Fig. 5 shows the fractional-PRF DOPCEN estimates, along with a straight line fit (it has been found that DOPCEN estimates are typically linear with azimuth time, over periods of tens of seconds). The next three panels of Fig. 5 show: the block rms value; how close the magnitude spectrum fits the expected high-SNR shape; the max/min ratio of the spectra in dB (almost the same as the "goodness of fit" curve); and the range and azimuth gradients.

The following points can be observed in this typical data set:

- The estimates conform well to the expected linear behaviour with azimuth time, except where the data undergoes substantial azimuth discontinuities. The discontinuities can be observed in the second and fourth panels (solid line) of Fig. 5, in the top panel of Fig. 3, as well as in the image itself, Fig. 2.
- The estimates taken in the low-energy water regions seem to be quite good despite the lower SNR and the poor spectral fit. See rows 10 to 13 and 22 to 26. The poor fit is due to the high noise floor, but the symmetry of the spectrum still yields good estimates.
- The AGC change around rows 16 and 17 does not affect the estimator appreciably in this case.

We ran similar tests on the other rows and columns of this scene. We also used the MLCC, DLR and MLBF estimators, and examined three RADARSAT-1 fine beam scenes with DOPCEN estimation difficulties. From this experience, we deduce that the azimuth radiometric gradient, as shown in the solid line in Fig. 5, is the best single predictor of poor estimator performance. We observe that if we can avoid the blocks which upset the estimators, a good global estimate can be made from the set of "good" blocks.

5 Global Fitting Strategy

Because we can recognize which blocks are likely to bias the DOPCEN estimate, and the estimates should be taken over as wide an area as possible, we propose a *global-fitting* algorithm based on the following strategy:

1. Use of spatial diversity:
    - Use as large an area as possible;

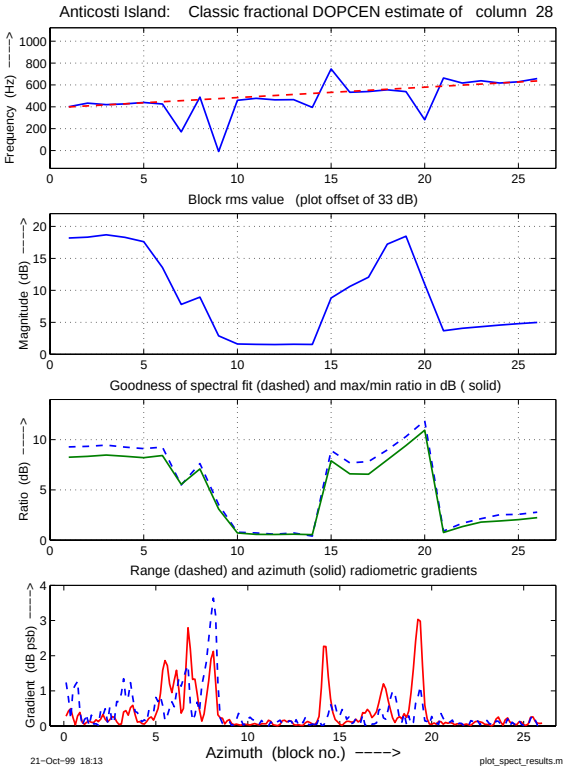

Figure 5: Summary of results of column 28 of the Anticosti scene.

- Divide the area into small blocks.

2. Reject blocks based on quality criteria such as:
   - scene statistics, and/or
   - estimator deviations.
3. Fit DOPCEN model globally over blocks:
   - constrain the fit to a sensible shape;
   - weight the blocks based on quality criteria.

The structure of the algorithm is outlined in Fig. 6. The key to the success of the algorithm is to begin with as large an area as possible, and to make a careful choice of the quality criteria used to exclude bad blocks from the final estimate (a mask is used to exclude bad blocks during the iterations). It was found best to begin by excluding blocks which had a higher than normal azimuth radiometric gradient, which ensures a reasonable initial fit, then finish by excluding additional blocks on a "worst-deviation" basis.

The maximum number of blocks that can be excluded is set to an upper limit, and if this number is exceeded, the iterations are redone with a different block size. Physical models for the Doppler based on the satellite attitude (along with the orbit and earth rotation) can be successfully used to predict the functional form of the DOPCEN curve [11, 12, 13], and constrain the estimate to a plausible shape.

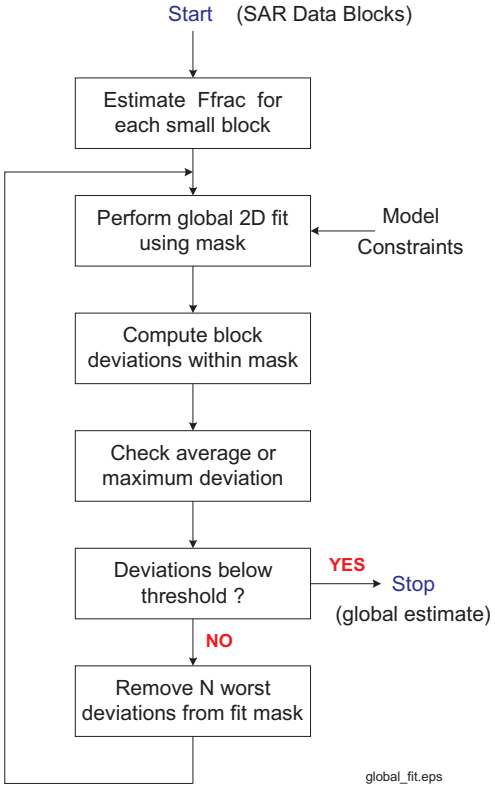

Figure 6: Global fit DOPCEN estimation algorithm.

5.1 Global fit results

The spectral fit estimator was run on blocks from every row and the results are shown in Fig. 7. The results of each block are reasonably smooth except when the azimuth gradient is large (compare Fig. 7 with Fig. 3).

We then applied the global fitting strategy of Fig. 6 with the bad blocks removed according to their azimuth gradient. More and more blocks are removed until the deviations from the fit of the remaining block estimates are less than a selected threshold (70 blocks of 728 were removed). For this scene, we recognized than the water areas had a Doppler bias (see below), and we also removed these from the global estimation. The following linear/quadratic fit was performed:

$$F_{DC} = \alpha_1 + \alpha_2\, a + \alpha_3\, r + \alpha_4\, r^2 \quad \text{Hz} \qquad (1)$$

where a is the azimuth block number centred on row 21.5 and r is the range block number centred on column 14.5. The fit coefficients are:

$$\alpha = [\,1415.3 \quad 8.4 \quad 34.4 \quad -0.07\,] \qquad (2)$$

and the result is shown in Fig. 8. Fig. 9 shows the deviations of each of the blocks from the fitted surface. Examining the 66 "good" blocks near the middle of Anticosti Island, the bias between the fitted surface and the 66 blocks is 0.006 Hz, and the rms deviation is 7.3 Hz. In the top 4 rows (112 blocks covering the northern mainland area), the bias between the fitted surface and the 66 blocks is -0.03 Hz, and the rms deviation is 12.7 Hz.

Note that the deviations shown in Fig. 9 do not directly relate to the error in the global fit. However, if the functional form of the fit is correct (i.e. the linear and quadratic terms are correct), and the block estimates are uncorrelated and unbiased, then the standard deviation of the global fit would be $1/\sqrt{N}$, when N blocks are used in the fit. Using this line of reasoning, we can say the small block deviations observed suggest that the global fit is likely good to 5 Hz or better over the land area.

An interesting observation is that there is a small bias of 35 Hz in the river area south-west of the island, which could be attributed to a current of 1.5 m/s. A smaller bias of 18 Hz exists in the water area in the centre right of the scene, presumably where the current is less. Other investigations [14, 2] suggest this is reasonable.

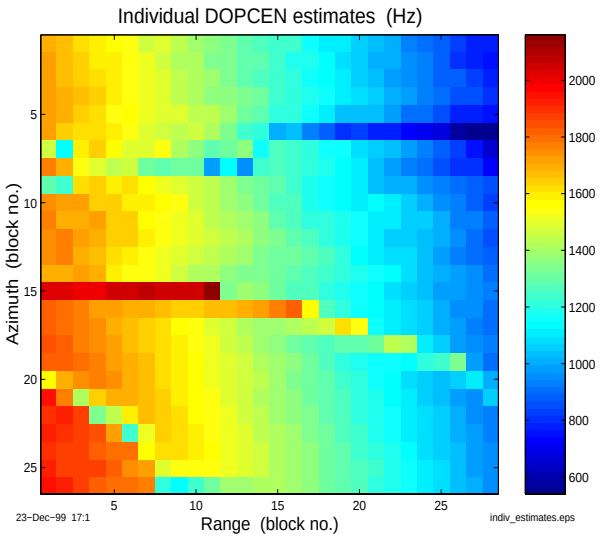

Figure 7: Individual DOPCEN estimates of each block.

6 Conclusions

In this paper, we have worked on the problem of bad DOPCEN estimates in RADARSAT-1 scenes. These occur most often when the radar passes over prolonged scene features where there is a prominent

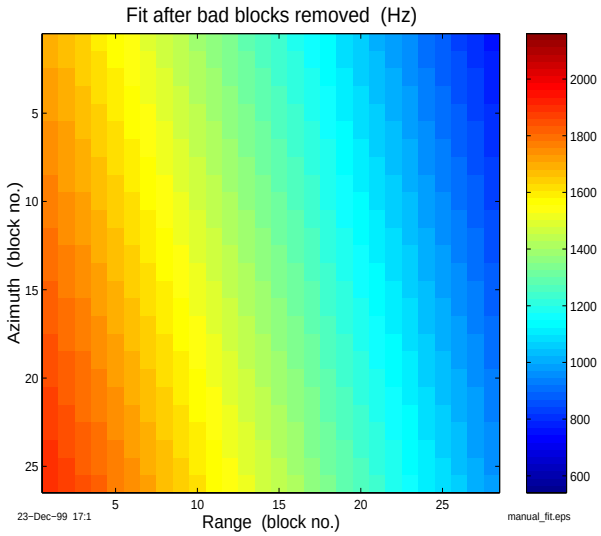

Figure 8: Quadratic surface fitted to good block estimates.

change in radiometry, as often happens on land/sea boundaries.

We have taken the approach of finding out what scene features upset the estimators most, and designing a global estimation scheme which excludes areas of the scene which cause bad estimates. The key to success of the algorithm is to work with as large an area as possible, and to choose a quality criteria which reliably identifies the bad blocks. There may also be a requirement to use adaptive methods where local altitude [15] or currents [2] may exist.

The algorithm is ideally suited to ScanSAR data, because of the large area available to the estimator. The large area increases the probability that bad areas can be avoided by the estimator. Also, ScanSAR has particularly demanding DOPCEN accuracy requirements, and we have shown that the global fit estimator shows the promise of meeting the ScanSAR estimation requirements of 5 Hz.

Acknowledgements

The authors would like to acknowledge the assistance of Kevin Murnaghan in providing some results from one of the CCRS standard processors; Julius Princz for providing range compressed data from the standard 'raw' product from the CDPF processor; Tommy Zhang of UBC for performing the simulation experiments; Bill Jefferies of RADARSAT International for supplying the raw data which were used in the study; and Paris Vachon for reviewing the manuscript. Funding to support this research came from a number of sources including the RSDDP pro-

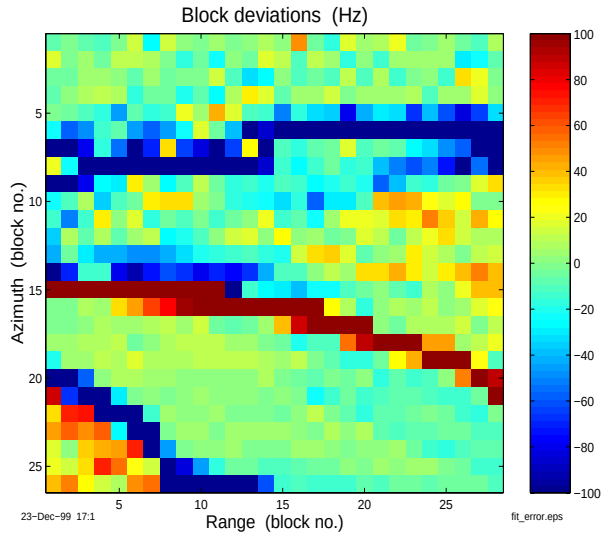

Figure 9: Deviations of individual estimates from quadratic fit (expanded scale).

gram, CSA, CCRS and MacDonald Dettwiler, and we are grateful for their support.

References

[1] R. K. Hawkins, T. I. Lukowski, K. P. Murnaghan, and S. K. Srivastava, "The effects of Doppler processing errors in SAR Data," in *Proc. of the CEOS SAR Calibration Workshop*, (Noordwijk, The Netherlands), pp. 201–208, February 2–5, 1998.

[2] D. C. Lancashire, "ScanSAR Calibration," in *Proc. of the CEOS SAR Calibration Workshop*, (Noordwijk, The Netherlands), pp. 241–245, February 2–5, 1998.

[3] S. N. Madsen, "Estimating the Doppler Centroid of SAR Data," *IEEE Trans. Aerospace and Electronic Systems*, vol. AES-25, pp. 134–140, Mar. 1989.

[4] R. Bamler and H. Runge, "PRF Ambiguity Resolving by Wavelength Diversity," *IEEE Trans. on Geoscience and Remote Sensing*, vol. 29, pp. 997–1003, Nov. 1991.

[5] F. H. Wong and I. G. Cumming, "A Combined SAR Doppler Estimation Scheme Based Upon Signal Phase," *IEEE Trans. on Geoscience and Remote Sensing*, vol. 34, pp. 696–707, May 1996.

[6] J. R. Bennett and I. G. Cumming, "A Digital Processor for the Production of SEASAT SAR Imagery," in *SURGE Workshop, ESA Publication SP-154*, (Frascati, Italy), July 16–18, 1979.

[7] F. K. Li, D. N. Held, J. Curlander, and C. Wu, "Doppler Parameter Estimation for Spaceborne Synthetic Aperture Radars," *IEEE Trans. on Geoscience and Remote Sensing*, vol. 23, pp. 47–56, Jan. 1985.

[8] F. H. Wong, I. G. Cumming, and R. A. Deane, "Doppler Ambiguity Resolver Based on Beat Frequency Between Range Looks," in *Proceedings of the Progress in Electromagnetics Research Symposium, PIERS'96*, (Innsbruck, Austria), p. 544 (abstract only), July 8–12, 1996.

[9] P. W. Vachon, A. L. Gray, C. E. Livingstone, and A. P. Luscombe, "Adaptive compensation of RADARSAT SAR analogue-to-digital converter saturation power loss," in *Proceedings of GER'97 (on CD-ROM)*, (Ottawa, Canada), May 27–29, 1997.

[10] T. Zhang, "Investigation of Biases in Doppler Centroid Estimation Algorithms," Master's thesis, Dept. of Electrical and Computer Engineering, The University of British Columbia, Aug. 1999.

[11] M. Dragošević, "On Accuracy of Attitude Estimation and Doppler Tracking," in *Proc. of the CEOS SAR Workshop*, (Toulouse, France, paper #164), October 26–29 1999. http://www.estec.esa.nl/CONFANNOUN/99b02/.

[12] V. Mitrovic, "RADARSAT CDPF single beam Doppler centroid estimation," Tech. Rep. RZ-TN-50-8357, MacDonald Dettwiler, Richmond, BC, Canada, 1997.

[13] S. R. Marandi, "RADARSAT attitude estimates based on Doppler centroid measurements," in *Proceedings of a Workshop on RADARSAT Data Quality*, (St. Hubert, Quebec, Canada), February 4–6, 1997.

[14] M. van der Kooij, W. Hughes, and S. Sato, "Doppler derived measurements of current velocity from spaceborne SAR data," *Can. J. Remote Sensing*, Submitted 1999.

[15] G. W. Davidson and I. G. Cumming, "Signal Properties of Squint Mode SAR," *IEEE Trans. on Geoscience and Remote Sensing*, vol. 35, pp. pp. 611–617, May 1997.